Critical Assessment of a Transitional Delayed Detached-Eddy Simulation Model for the Prediction of the Linear Compressor Cascade V103

Felix M. Möller*
German Aerospace Center (DLR), Cologne, Germany

Paul G. Tucker†
University of Cambridge, Cambridge, United Kingdom

Zhong-Nan Wang‡
University of Birmingham, Birmingham, United Kingdom

Christian Morsbach§
German Aerospace Center (DLR), Cologne, Germany

The accurate prediction of transitional flows is crucial for the industrial turbomachinery design process. While RANS inherently brings conceptual weaknesses, LES will be still too expensive in the near future to affordably simulate complex turbomachinery configurations. We introduce a transitional DDES model, namely DDES-γ, and analyze numerical results of the compressor cascade V103. A comparison with the fully turbulent DDES approach emphasizes the benefit of coupling DDES with a transition model. Issues with undesired decay of modelled turbulent kinetic energy in the free-stream are improved when running DDES-γ in combination with the synthetic turbulence generator method. Best results for DDES-γ are obtained when changing the inviscid flux solver blending from dynamic to constant mode. We show that DDES-γ is capable to predict the transitional flow through a linear compressor cascade, but also critically discuss the general concept and results.

I. Introduction

Covering laminar-to-turbulent transition with modern CFD methods is of big importance for an accurate turbomachinery design process. The development of pure Reynolds-averaged Navier-Stokes (RANS) transition models is still an ongoing research field. Nevertheless, weaknesses coming from the RANS approach itself yield limitations in the predictive quality of steady RANS simulations. On the other hand, the large-eddy simulation (LES) method can be used to accurately predict the transition process (see e.g. Lardeau et al. [1], Marty [2] or Scillitoe et al. [3]). Since the computational effort of LES scales with the Reynolds number, it is still expensive (or rather impossible) to simulate realistic turbomachinery configurations in the industrial design process. To benefit from both worlds, seamless hybrid RANS/LES (HRL) methods have been introduced. Their motivation is to utilize a RANS model in regions where RANS is capable to determine accurate results. In regions where RANS models fail, HRL methods should switch to an LES-mode to resolve turbulent scales and ensure high predictive quality. Whilst the main focus of development for the last decades has been on fully turbulent flows, it is important to also deal with transitional flows, especially for turbomachinery applications. Hence, the prediction of transitional flows with HRL methods, such as delayed detached-eddy simulation (DDES), has been received more attention, recently.

To the author's knowledge, Magagnato et al. [4] were the first who assessed the predictive quality of the original detached-eddy simulation (DES) model (Spalart et al. [5]) for transitional flows in a VKI turbine cascade without utilizing an additional transition model. Numerical results were '*less satisfactory*' [4], which can be seen as expectable when running a model designed for fully turbulent flows in transitional circumstances. Wang et al. [6] first mentioned

*Research Associate, Institute of Test and Simulation for Gas Turbines, felix.moeller@dlr.de, 51147 Cologne, Germany
†Rank Professor of Engineering, Department of Engineering, Cambridge, CB2 1PZ, United Kingdom
‡Lecturer (Assistant Professor) in Aerospace, College of Engineering and Physical Sciences, Birmingham, B15 2TT, United Kingdom
§Team Leader, Institute of Propulsion Technology, 51147 Cologne, Germany

the potential of coupling a RANS transition model with the DES framework after they introduced a modular RANS transition model based on an additional transport equation for the intermittency factor γ. This model has been reworked in the HRL context and published by Wang et al. [7] which illustrates improved results and the capability of predicting transitional flows with the DDES model on a highly loaded Controlled Diffusion Airfoil (CDA). Xiao et al. [8] also proposed the coupling of the classical DDES model with a one-equation γ-transition model (introduced by Wang and Fu [9]) and computed the flow past the Orion capsule. Sørensen et al. [10] and Sa et al. [11] coupled a DES model with the two-equation γ-Re_θ transition model and also showed improved results in the prediction of the transition process. They illustrated the improvements with the circular cylinder, the DU-96-W-351 airfoil and the Eppler 387 airfoil. Alam et al. [12] proposed another concept which is based on the three-equation k-k_l-ω model by Walters et al. [13]. The beneficial prediction of the transition process on the surface of the PAK-B airfoil is also confirmed by their coupled model. Yin et al. [14] introduced a transitional DDES model based on the adaptive l^2-ω model, with whom they obtained improved results for the computation of the T3 ERCOFTAC flat plate series. This trend has been confirmed with their simulation of the compressor cascade V103 in Yin and Durbin [15]. The big variety of different approaches emphasizes the importance of this research field, but one unified concept could not be found yet.

Since the DDES model is mainly designed for massively separated flows, the most obvious transition type to consider is separation-induced transition. This is why we introduced a way to couple the DDES with the γ-transition model (DDES-γ) and assessed the predictive quality for separation-induced transition in [16]. Besides separation-induced transition, Mayle [17] further introduced natural transition, bypass transition and wake-induced transition as main types occurring in turbomachinery flows. While natural transition can be neglected in turbomachinery due to increased free-stream turbulence intensity (FSTI), the latter two transition types play an important role. After assessing separation-induced transition stand-alone (cf. [16]), it is a next logical step, to consider cases including bypass transition. Certainly, wake-induced transition is of big importance, especially, when simulating multi-row and multi-stage configurations, but this will be focus of future work. To assess the coupled DDES-γ model, we choose the compressor cascade V103 which is a linear cascade based on the NACA-65 profile and features separation-induced transition on the suction side and bypass transition on the pressure side.

In this paper, we discuss the concept of coupling the DDES model with the correlation-based γ-transition model to predict transitional flows. Before analyzing physical results of the flow through the compressor cascade V103, the model itself and respective switches and functions will be discussed in Sec. II. These relations will help to judge computational results of the compressor cascade V103 in Sec. III. Eventually, our results will be summarized in Sec. IV.

II. Methodology

A. Turbulence and transition model

1. DDES model

The utilized DDES model is based on the two-equation Menter-SST turbulence model (see Travin et al. [18]). The 'hybridization' of any RANS turbulence model is realized by modifying the destruction term D_k in the k-transport equation. For the Menter-SST model, this transport equation is defined as

$$\frac{\partial}{\partial t}(\rho k) + \frac{\partial}{\partial x_j}(\rho u_j k) = \tilde{P}_k - D_k + \frac{\partial}{\partial x_j}\left[(\mu + \sigma_k \mu_t)\,\frac{\partial k}{\partial x_j}\right] \tag{1}$$

The destruction term can be expressed as a function of a model-specific length scale

$$D_k = \frac{\rho k^{3/2}}{l_{\mathrm{DDES}}} \tag{2}$$

which, for the DDES model, is defined as

$$l_{\mathrm{DDES}} = l_{\mathrm{RANS}} - f_d \max\left(0, l_{\mathrm{RANS}} - C_{\mathrm{DES}}\Delta_{\mathrm{SLS}}\right) \tag{3}$$

with the sub-grid length scale (SLS) Δ_{SLS} and $C_{\mathrm{DES}} = 0.65$. For $f_d = 0$ or $l_{\mathrm{RANS}} < C_{\mathrm{DES}}\Delta_{\mathrm{SLS}}$, this length scale reduces to the original RANS length scale and RANS model behavior is expected. The boundary layer shielding function f_d, introduced by Spalart et al. [19], is in charge of preventing LES-mode in a boundary layer, where the resolution is not

capable to handle resolved scales properly, as this would yield unphysical results due to modelled stress depletion (MSD) and grid-induced separation (GIS) ([19], [20]). The shielding is defined as

$$f_d = 1 - \tanh\left[(C_{d1} r_d)^{C_{d2}}\right] \tag{4}$$

where $C_{d2} = 3$ follows the original proposal of [19] and $C_{d1} = 20$ is in alignment with the investigations of Gritskevich et al. [20], focusing on the coupling of DDES with the Menter-SST model. The parameter r_d is given by

$$r_d = \frac{\nu_t + \nu}{\sqrt{u_{i,j} u_{i,j}}\kappa^2 d^2} \tag{5}$$

with the eddy viscosity ν_t and the kinematic viscosity ν, the velocity gradients $u_{i,j}$, the Kármán constant κ and the distance to the wall d. The shielding function f_d must be considered as an 'enabler' for the LES-mode. It actively shields regions of the domain and prevents the LES-mode ($f_d = 0$), but does not actually activate this mode. The LES-mode is only activated, if $l_{\mathrm{RANS}} > C_{\mathrm{DES}}\Delta_{\mathrm{SLS}}$ and $f_d \neq 0$.

The required Δ_{SLS} was initially introduced based on the mesh by Spalart et al. [5]. New approaches (cf. [21], [22], [23]) improved this length scale and nowadays also incorporate flow physics, such as the vorticity vector. The simulations in the present paper are based on the extended, vorticity-based Δ_{SLA} (= **s**hear **l**ayer **a**daptive) by Shur et al. [24]. A detailed explanation of the determination can be found in [24]. In the following, when we write Δ_{SLS}, the SLS approach by Shur et al. is meant.

To easily distinguish between RANS- and LES-mode, the length scale ratio is often used:

$$l_{\mathrm{ratio}} = \frac{l_{\mathrm{RANS}}}{l_{\mathrm{DDES}}} \tag{6}$$

In RANS regions, this ratio is equal to unity, because Eq. (3) yields $l_{\mathrm{DDES}} = l_{\mathrm{RANS}}$. In LES regions, it is greater than unity. Increasing l_{ratio} values express a stronger modification of the k-transport equation in terms of a stronger reduction of modelled turbulent kinetic energy (TKE). l_{ratio} values smaller than unity are not possible for the DDES model. This simple differentiation between RANS- and LES-mode for transitional cases will be critically discussed.

2. γ-transition model

The transition model to be coupled with the fully turbulent DDES model is the one-equation γ-transition model, introduced by Menter et al. [25]. The γ-transport equation is defined as follows

$$\frac{\partial}{\partial t}(\rho\gamma) + \frac{\partial}{\partial x_j}(\rho u_j \gamma) = P_\gamma - D_\gamma + \frac{\partial}{\partial x_j}\left[\left(\mu + \frac{\mu_t}{\sigma_\gamma}\right)\frac{\partial \gamma}{\partial x_j}\right] \tag{7}$$

Details about the single terms and how the second transport equation for Re_θ is reduced to a functional expression can be found in [25]. We decided for the one-equation transition model, because the reduced number of transport equations also yields reduced computational effort, which will be of importance when simulating larger configurations with DDES-γ. Further, the reported Galilean invariant model formulation (cf. [25]) is seen as an additional strength in comparison to the widely-used γ-Re_θ transition model.

3. Coupled DDES-γ model

The coupling for the RANS Menter-SST model is also well-described in [25]. The computed γ from Eq. (7) is integrated into the original k-transport equation, which finally yields a modified transport equation

$$\frac{\partial}{\partial t}(\rho k) + \frac{\partial}{\partial x_j}(\rho u_j k) = \tilde{P}_{k,\mathrm{trans}} + \cancel{P_k^{\mathrm{lim}}} - D_{k,\mathrm{trans}} + \frac{\partial}{\partial x_j}\left[(\mu + \sigma_k \mu_t)\frac{\partial k}{\partial x_j}\right] \tag{8}$$

with $\tilde{P}_{k,\mathrm{trans}} = \gamma \tilde{P}_k$ and $D_{k,\mathrm{trans}} = \max(0.1, \gamma) D_k$. The additionally proposed production term P_k^{lim} was intended for RANS simulations to accelerate the transition process in separated shear layers [25], but needs to be eliminated for a coupled DDES-γ model [16]. Merging the destruction term of the fully turbulent DDES (cf. Eq. (2)) and the modified destruction term from the transition model coupling, we obtain

$$D_{k,\mathrm{trans}} = \max(0.1, \gamma)\frac{\rho k^{3/2}}{l_{\mathrm{DDES}}}. \tag{9}$$

This redefined destruction term (Eq. (9)) and the elimination of P_k^{lim} in Eq. (8) build the foundation of the coupled DDES-γ model.

B. Numerical solver blending

For the fully turbulent DDES model, Travin et al. [18] proposed a *dynamic* solver blending factor σ_b, which, for the Riemann solver, switches between a central and an upwind (cf. Roe [26]) formulation to compute the inviscid fluxes F_{inv}. It is the model's intention to decide inherently where to use the dissipative upwind flux F_{upwind} (desired in RANS/attached regions, to ensure a stable RANS-mode) and where to utilize a central flux F_{central} (desired in LES/separated regions, to facilitate the development of physical instabilities). The blending between these two formulations is realized with

$$F_{\text{inv}} = (1 - \sigma_b) F_{\text{central}} + \sigma_b F_{\text{upwind}} \tag{10}$$

A detailed description of σ_b and its computation can be found in [18].

Another approach of 'blending' between inviscid central and upwind fluxes can be realized by a *constant* solver blending. It differs conceptually to the *dynamic* blending, that it defines a constant amount of upwind flux in each cell, meaning σ_b (cf. Eq. (10)) is a user-defined constant factor. In Sec. III.B.3, we will also discuss results for a *constant* solver blending and work out physical differences in comparison to the *dynamic* blending.

C. Interaction of different model switches

After introducing all relevant model equations and parameters separately in the previous subsections, we discuss and illustrate the interactions theoretically, before interpreting numerical results. Relevant model parameters of DDES-γ are:

1) RANS length scale l_{RANS}
2) Sub-grid length scale Δ_{SLS}
3) Shielding function f_d
4) Intermittency factor γ
5) Solver blending σ_b

The destruction term for our coupled DDES-γ model (cf. Eq. (9)) can be reformulated, so that the parameters 1) - 4) are visible in a single term:

$$D_{k,\text{trans}} = \max(0.1, \gamma) \frac{\rho k^{3/2}}{l_{\text{RANS}} - f_d \max\left(0, l_{\text{RANS}} - C_{\text{DES}} \Delta_{\text{SLS}}\right)} \tag{11}$$

Based on this expression the hierarchy of model values can be illustrated. Fig. 1 depicts schematics for the two different model configurations (fully turbulent and transitional). Assuming a fully turbulent setup, γ would be equal to unity. This configuration is illustrated in Fig. 1a. In the initial RANS region (①), modelled TKE is produced, leading to high k_{mod} values prior to separation occur. At the separation onset (②), a comparison of l_{RANS} and Δ_{SLS} is fair, since increased l_{RANS} values allow the activation of LES-mode via the denominator in Eq. (11). The increased destruction term yields an active reduction of modelled TKE in this region. After reattachment, the model is designed to switch from LES- to RANS-region (③). In short, the differentiation between RANS- and LES-mode for fully turbulent flows is sensible and easy to realize by comparing the respective length scales.

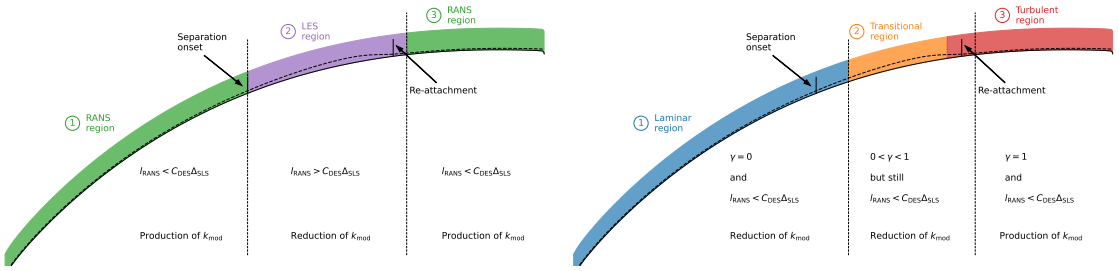

(a) Fully turbulent DDES **(b) Transitional DDES**

Fig. 1 Schematics of different model configurations and flow regions. Separation streamline is depicted as black dashed line.

The main differences between fully turbulent and transitional cases is the state prior to separation. In contrast to the fully turbulent case, no significant k_{mod} is present in the transitional case. Fig. 1b illustrates the schematics of a transitional blade flow. The clear classification of RANS and LES regions is not possible anymore. For transitional

cases, γ equals zero in the laminar region (Fig. 1b ①), which yields $\tilde{P}_{k,\text{trans}} = 0$ and $D_{k,\text{trans}}$ is equal to 10 % of the original destruction. As a consequence, modelled TKE is kept to a minimum, thus, also the RANS length scale is almost zero. The typical comparison of l_{RANS} and Δ_{SLS} is not sensible anymore, since the 'LES-mode' (meaning $l_{\text{RANS}} > C_{\text{DES}}\Delta_{\text{SLS}}$) would only be possible with extremely fine meshes. For transitional cases, very small RANS length scales will always be greater than a sub-grid length scale, resulting in a declaration of a RANS-mode, although it is more a laminar mode, where no turbulence is produced. Even in the transitional region (see Fig. 1b ②) l_{RANS} is very small due to initially small γ-values which hinder the RANS length scale to grow. After γ reaches unity, the original intention of the DDES model takes over and increasing modelled TKE is immediately reduced by manipulating the k-destruction term.

In laminar regions, the DDES-γ acts more like an implicit LES. The sub-grid (modelled) viscosity is kept to a minimum and the model attempts to resolve turbulent scales, which explains the higher demand on the mesh resolution. This aspect needs to be remembered when we discuss our numerical setup and results in Sec. III.

Eventually, the *dynamic* solver blending σ_b is considered. From the previous discussion, we learnt, that a classical differentiation between RANS- and LES-region is not sensible anymore for transitional cases. Since the *dynamic* solver blending was designed for fully turbulent circumstances, the clear distinction between RANS- and LES-mode is also part of this blending approach (as described in Sec. II.B).

It is important to remember this discussion, when we analyze the transitional flow through the compressor cascade V103.

D. Synthetic inflow turbulence

We conducted also simulations with the synthetic turbulence generator (STG) method (cf. Sec. III.B.2 and Sec. III.B.3) proposed by Shur et al. [27]. This method has been implemented and validated in *TRACE*[*] by Morsbach and Franke [28]. Further analysis was done by Matha et al. [29]. We omit discussing the STG model in detail at this point, since this is not focus of our work. Detailed information about the numerical STG settings will be given in Sec. III.A.

E. Comment on basis validation for bypass transition

We analyzed the model behavior of DDES-γ for separation-induced transition with canonical and turbomachinery test cases in [16]. Before we assess the compressor cascade in Sec. III, we considered the T3C5 flat plate case from ERCOFTAC database[†] to validate the behavior of DDES-γ for pure bypass transition with a canonical test case. The FSTI of the T3C5 case is comparable to the compressor cascade analyzed in the following section which is why we picked this special case. The DDES-γ model showed identical results in comparison with the respective RANS-γ formulation. This was expected (or rather desired) since in attached transitional boundary layers we do not expect improvements by DDES-γ ultimately and the coupling does not worsen results. At this point, we resign to illustrate numerical results, because a comparison RANS-γ and DDES-γ revealed identical results for this plain test case. In the following section, we assess how the DDES-γ model acts for bypass transition in a more complex configuration.

III. Linear compressor cascade V103

After we introduced the DDES-γ model and discussed interactions and differences to fully turbulent modelling approaches theoretically in the previous section, we will now assess the DDES models in a transitional flow through a compressor cascade. This test case was experimentally considered by Hilgenfeld and Pfitzner [30]. The operating conditions (Ma = 0.67 and Re = 450 000) would have been too challenging for a direct numerical simulation (DNS), which is why Zaki et al. [31] decided to scale this case. Their DNS simulation serves as a numerical reference to better assess the results of DDES-γ. In the following, we first introduce the numerical setup, before we analyze DDES results. Where actual data is available, we always put our results into relation to other research groups.

A. Numerical setup

We consider the scaled operating point also simulated by Zaki et al. [31]. This results in an inflow Mach number Ma = 0.1 and a Reynolds number Re = 138 500, based on the axial chord length $c_{\text{ax}} = 0.204$ m and the bulk inflow velocity U_0. Characteristic parameters of the cascade are summarized in Table 1. The span size of $0.1c_{\text{ax}}$ is also used by

[*] TRACE User Guide

[†] ERCOFTAC database: Flat Plate Transitional Boundary Layers

Table 1 Overview of considered operating point and geometrical parameters.

Flow parameters	
Reynolds number Re	138 500
Mach number Ma	0.1
Inflow turbulence intensity TI	3.25 %
Inflow angle	42°
Geometrical parameters	
Axial chord length c_{ax}	0.204 m
Pitch y	0.12036 m
Span h	$0.1c_{ax}$

other research groups. An analysis of the two-point correlation confirms, that the spanwise extent is sufficient to properly capture turbulent coherent structures, which is the case when uncorrelated time signals occur in spanwise direction.

Fig. 2 illustrates the computational domain. At the inlet (at $x/c_{ax} = -0.4$, marked with green vertical line), we either prescribe modelled turbulence via TI = 3.25 % and the turbulent length scale $l_t = 0.003c_{ax}$ or we utilize the STG for the prescription of resolved turbulence. Therefore, we extract a bulk state from the RANS precursor simulation and provide the velocity vector, density and static pressure for the STG to compute the inlet boundary condition for resolved turbulence. Additionally, the length scale is increased to $l_t = 0.055c_{ax}$. Differences in the l_t value for simulations without and with STG are explicable with the different definition of inflow boundary condition. For simulations with the STG, we follow the proposed inlet boundary condition of Shur et al. [27] where the inlet turbulent dissipation rate is defined as follows

$$\omega_{\text{inlet}} = \frac{\sqrt{k}}{\beta_k l_t} \tag{12}$$

with $\beta_k = 0.09$. This constant is not used, when determining ω_{inlet} for simulations without the STG. To ensure a comparable inlet turbulent dissipation rate, we need to increase l_t for the STG simulation. At the outlet panel (at $x/c_{ax} = 1.4$, marked with red vertical line), we prescribe a constant static back pressure, which was iteratively determined

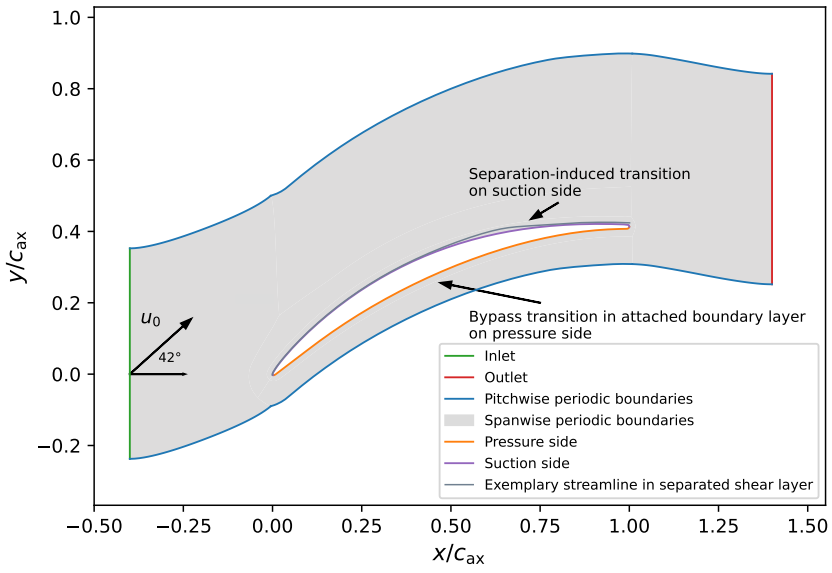

Fig. 2 Schematics of the numerical domain for the compressor cascade V103.

until the pressure distribution of the DNS reference data was met with acceptable accuracy. For the introduced operating point (cf. Table 1), on the suction side, separation-induced transition occurs. On the pressure side, bypass transition can be observed. The simultaneous appearance of two transition types is a challenging setup for the DDES-γ model, which motivates the assessment of this case.

Our DDES mesh setup is in close agreement with the one by Yin and Durbin [15]. We also varied the mesh density by coarsening and refining the resolution. The coarser setup yielded increasing deviations whereas the refined mesh did not show remarkable improvements, which is why we choose a mesh resolution (summarized in Table 2) for further analysis in this work. In addition, a summary of respective mesh resolutions for different simulations types and research groups can be found in Table 2. To obtain further reaching reference data, we also conducted an LES simulation. This LES simulation was conducted with the WALE sub-grid model proposed by Nicoud and Ducros [32].

Table 2 Overview of generated meshes and comparison to other research groups.

Simulation type	Authors	Total number of cells
DDES	Present paper	1 079 440
LES		10 859 760
DDES	Yin and Durbin [15]	1 474 560
LES	Lardeau et al. [1]	6 291 456
LES	Scillitoe et al. [3]	9 300 000
DNS	Zaki et al. [31]	83 886 080

All simulations have been carried out with the DLR in-house solver *TRACE*[‡] which is developed at the Institute of Propulsion Technology in the Department for Numerical Methods with special focus on turbomachinery applications. We employed the density-based cell-centered finite-volume solver of *TRACE*. The accuracy for the spatial discretization is of 2$^{\text{nd}}$-order with an additional inviscid flux blending, explained in Sec. II.B. The temporal discretization is realized with a 3$^{\text{rd}}$-order explicit Runge-Kutta method.

B. Results

In the following, we assess computational results of the coupled DDES-γ. All third-party references will be illustrated with symbols (○). Own LES reference data is presented with a solid black line (—). The simulation has been conducted for the effective number of $t/t_c = 11.5$ through flows, with the convective time $t_c = c_{\text{ax}}/u_0$. For all DDES simulations, we ensure a simulation duration of $t/t_c = 37$.

1. Comparison of baseline DDES-γ and DDES-FT

As a starting point, we consider the baseline DDES setup and compare results of the fully turbulent (FT) model with those of DDES-γ. This setup uses a *dynamic* solver blending and *no STG* and is more oriented towards a typical steady RANS setup. Main motivation for this comparison is to highlight differences between a transitional RANS, fully turbulent DDES and the transitional DDES-γ model.

We begin with the analysis of the pressure distribution c_p along the blade surface in Fig. 3 to assess the global match of the operation point. Besides our DDES results, we compare with DNS [31], RANS [25] and our own LES data. Generally, our LES and the DNS data show very good agreement. It becomes clear, that RANS-γ is not capable of accurately predicting the separation bubble size on the suction side, whereas deviations on the pressure side, with respect to DNS data, are not significant. The DDES-FT model fails to accurately predict the separation bubble on the suction side and deviations on the pressure increase from $x/c_{\text{ax}} \approx 0.5$. Generally, the operating point is slightly deviating which is apparent due to a changed pressure level at the trailing edge. On the other hand, the DDES-γ, with the baseline setup, already shows acceptable results. The separation bubble on the suction side, as well as the pressure side distribution are in reasonable agreement with LES and DNS data.

Focusing on the suction side, we illustrate the tangential velocity profiles prior to the separation in Fig. 4. It is well illustrated, that DDES-FT quickly deviates from numerical reference data. The fully turbulent modelling approach

[‡]TRACE User Guide

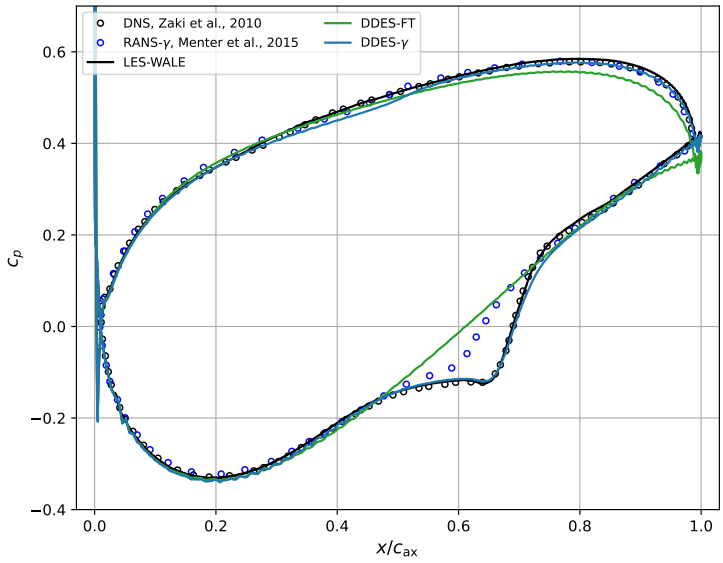

Fig. 3 Pressure distribution c_p along the blade surface.

yields premature increased modelled TKE in the boundary layer which does not represent the actual circumstances prior to the separation-induced transition. Our LES results are in very good alignment with the DNS reference data. The DDES-γ follows numerical references well, with acceptable deviations.

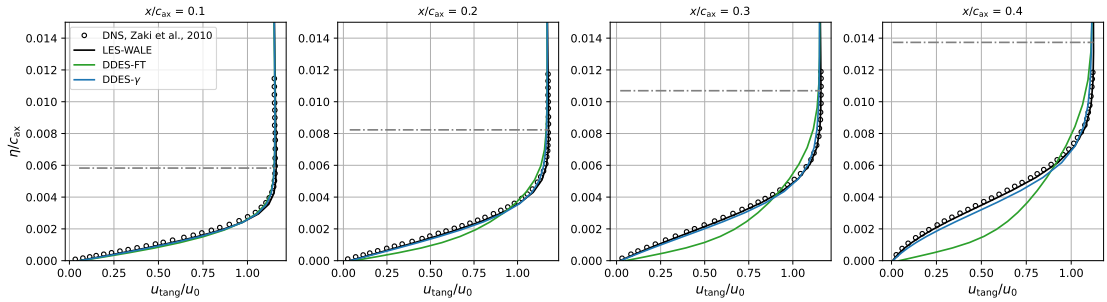

Fig. 4 Normalized tangential velocity profiles on the suction side prior to separation. Horizontal grey dash-dotted line marks the boundary layer edge for LES simulation.

To further assess the transition processes on the blade surface, we consider the friction coefficient c_f in Fig. 5. In addition to the previously shown reference data, we now add numerical DDES data by Yin and Durbin [15]. The suction (cf. Fig. 5a) and pressure side (cf. Fig. 5b) are shown separately. Focusing on the suction side, in Fig. 5a, the positive trend is confirmed. Whilst the fully turbulent DDES model does not capture the correct separation-induced transition process at all, DDES-γ shows already good agreement with the DNS reference data. Prior to the separation and also prior to transition (at $x/c_{ax} \approx 0.65$), DDES-γ is almost identical to the reference data. After the transition and reattachment, we observe deviations which can be explained with the help of wall-normal TKE boundary layer cuts in Fig. 6. For DDES-FT we see, that the modelled TKE (cf. Fig. 6a) is immediately high in the wall vicinity from first measurement station. Since for this comparison STG was not utilized, there is no resolved TKE for DDES-FT (cf. Fig. 6b). The premature production of k_{mod} suppresses the laminar separation bubble but leads to an open separation bubble close to the trailing edge, which is why the DDES model does not switch to a resolved mode and modelled TKE is never reduced. Overall, DDES-FT over-predicts the total level of TKE in the laminar region (cf. Fig. 6c) and lacks turbulence in the reattachment and turbulent region. For the DDES-γ model, in the laminar region ($x/c_{ax} < 0.6$) the modelled TKE is kept to a minimum by the coupled γ-transition model. Again, this simulation is conducted without

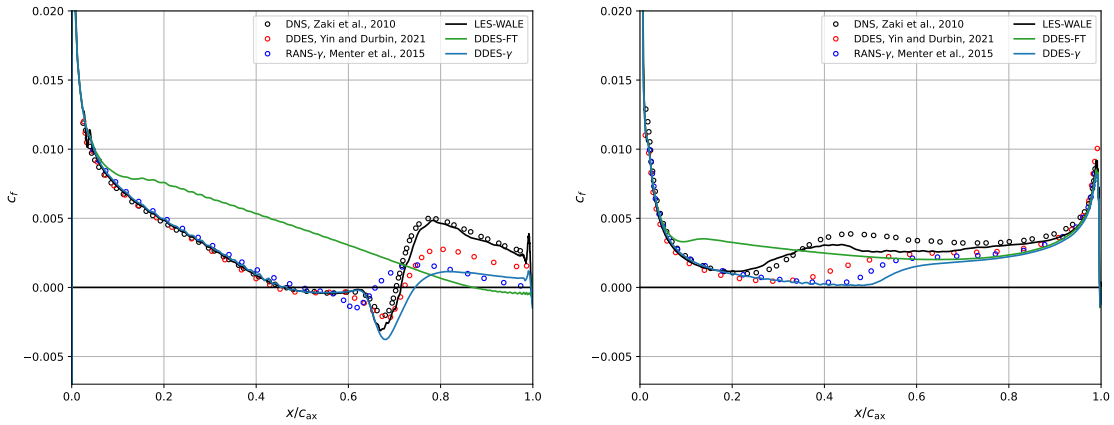

(a) Suction side **(b) Pressure side**

Fig. 5 Friction coefficient c_f along respective blade sides.

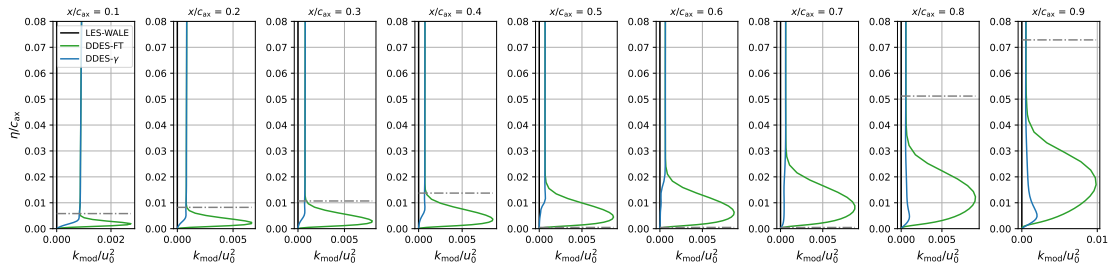

(a) Modelled turbulent kinetic energy

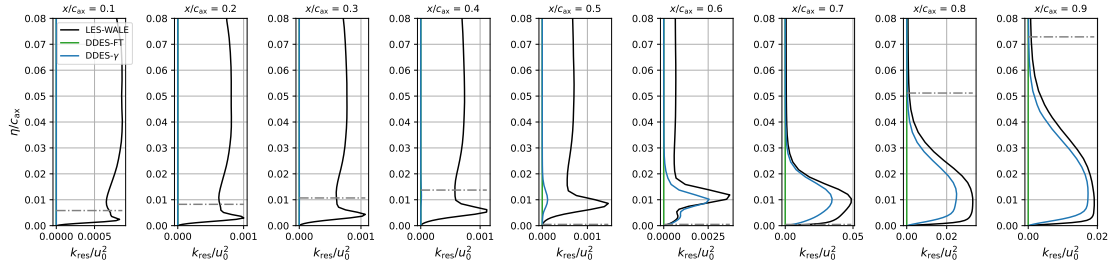

(b) Resolved turbulent kinetic energy

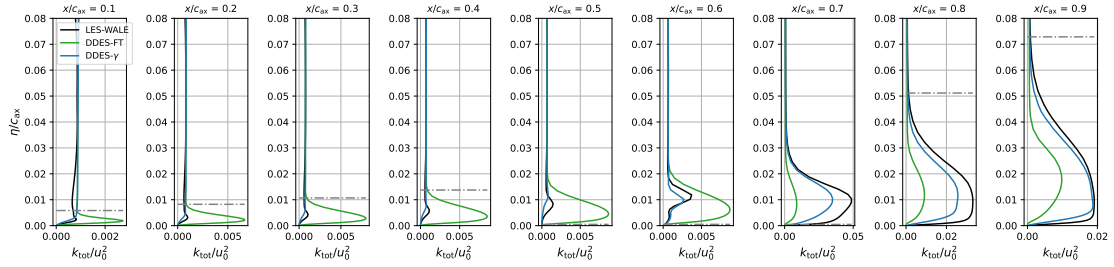

(c) Total turbulent kinetic energy

Fig. 6 Normalized wall-normal boundary layer cuts of the different TKE components along the suction side. Horizontal grey dash-dotted line depicts the boundary layer edge for our LES reference simulation.

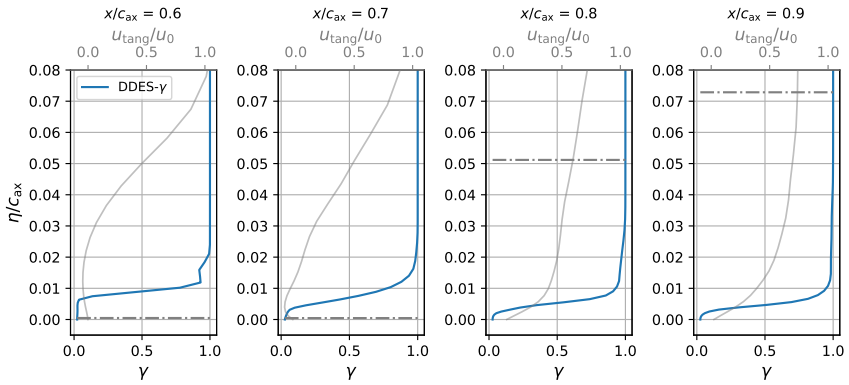

Fig. 7 Wall-normal intermittency γ profiles in the separated and post-reattachment region on the suction side. Horizontal grey dash-dotted line marks the determined boundary layer edge for LES simulation. Grey solid line illustrates the normalized tangential velocity profile of the LES simulation.

the STG which is why resolved TKE is also very low in the upstream stations of the suction side (cf. Fig. 6b between $0.1 \leq x/c_{ax} \leq 0.5$). In the separation bubble (at $x/c_{ax} = 0.6$), resolved content is in qualitative agreement with the LES. The low level of k_{mod} and the small gap of k_{res} between LES reference and DDES-γ after the reattachment explain the deviations in the friction coefficient in the reattachment region in Fig. 5a. The reduced turbulent state in the boundary layer yields reduced momentum which further leads to smaller velocity gradients. This is why c_f is under-predicted by DDES-γ in the reattachment region. A reasonable production of modelled TKE is affected from the underlying γ-model which prevents modelled content after the reattachment. To assess this, we illustrate γ-profiles for DDES-γ in the separated and post-reattachment region in Fig. 7. Especially the wall-closest region reveals γ close to zero, which hinders the production of k_{mod}.

Coming back to the friction coefficient, we now focus on the pressure side in Fig. 5b. The fully turbulent approach DDES-FT, again, is not capable of predicting the bypass transition process. A missing transition model yields unphysical production of modelled TKE and premature 'transition' immediately after the leading edge. For the bypass transition, DDES-γ results are more aligned with RANS-γ and do not follow the DNS reference data or DDES results of Yin and Durbin [15]. Massive improvements for the prediction of bypass transition are not expected by the baseline setup, because in attached boundary layers the DDES model should behave as a RANS model which is why we would expect more or less identical results to RANS-γ.

To support this statement, we show boundary layer cuts of l_{ratio} and γ in Fig. 8. In Fig. 8a, we learn, that the length scale ratio l_{ratio} rarely exceeds unity which is a constant RANS behavior on the blade pressure side. Without resolved content, we cannot expect any improvements of DDES-γ in comparison to RANS-γ. The minor deterioration by a slightly delayed transition onset can be explained when taking the intermittency factor (cf. Fig. 8b) into account. It becomes clear, that in the outer boundary layer ($\eta/c_{ax} > 0.1$), γ is equal to unity, which means in this region the underlying RANS model thrives to produce modelled TKE. On the contrary, the small increase of the length scale ratio recognizable between $0.4 \leq \eta/c_{ax} \leq 0.6$ means an undesired local reduction of the modelled TKE by the model which explains the missing modelled content to meet RANS-γ results and, thus, slightly deviating results for the prediction of bypass transition.

The beneficial behavior of DDES-γ in comparison to DDES-FT has become clear throughout the previously presented results. Nevertheless, the baseline DDES-γ setup (*dynamic* solver blending and *no* STG) also revealed weaknesses. Besides the minor deviation in the prediction of both transition types which could be explained by the model behavior, we now like to focus on the free-stream turbulence. Fig. 9 shows the total turbulence intensity along a streamline intersecting the leading edge mid-pitch position. The modelled and resolved turbulence intensity components are not illustrated separately at this point, because no STG was utilized and for RANS and DDES simulations, the total turbulence intensity is equal to the modelled ones. We illustrate the DNS reference data, but also LES results by Scillitoe et al. [3] and, again, RANS results. All these references and the conducted LES simulation follow the same trend. For both DDES results, another trend is apparent. Close to the leading edge plane, the turbulence intensity decreases rapidly. Since there is no resolved turbulence prescribed, this drop is, in fact, an unphysical drop in the modelled component.

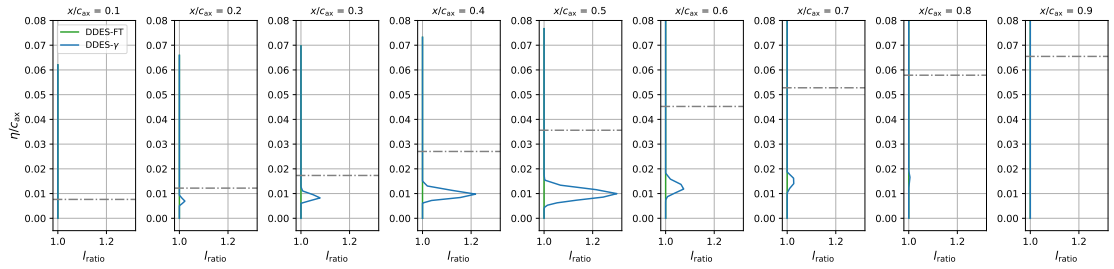

(a) Length scale ratio

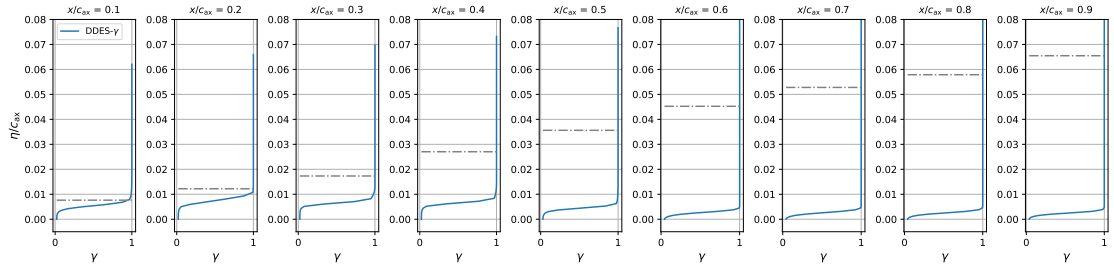

(b) Intermittency factor

Fig. 8 Wall-normal boundary layer cuts along the pressure side. Horizontal grey dash-dotted line depicts the boundary layer edge for our LES reference simulation.

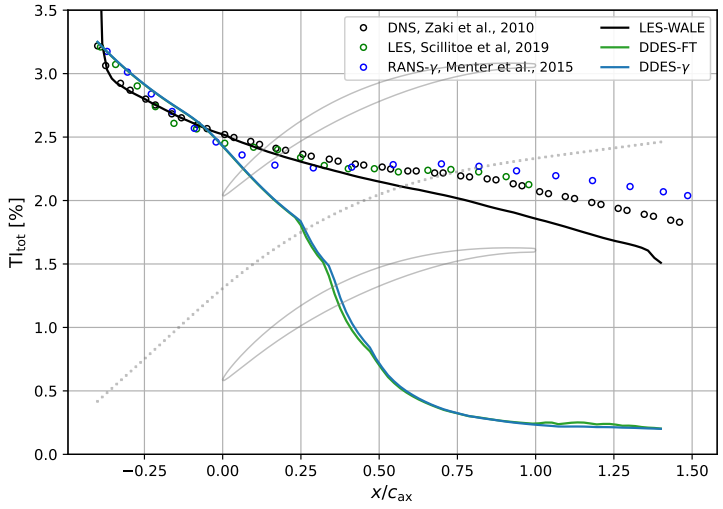

Fig. 9 Total turbulence intensity TI along extracted streamline intersecting the leading edge mid-pitch position (illustrated in the background with grey dots). For RANS and DDES simulations, the total TI is equivalent to modelled TI.

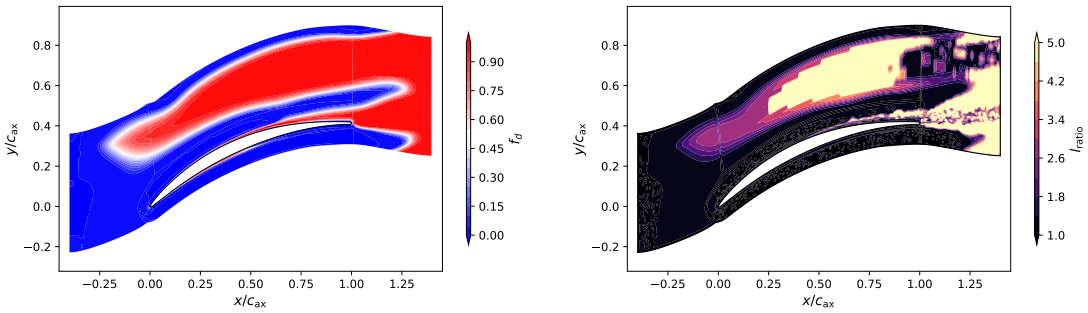

(a) Shielding function **(b) Length scale ratio**

Fig. 10 Time-averaged contour slices of spanwise-averaged variables for DDES-γ. In (a), $f_d = 0$ determines RANS-mode and $f_d > 0$ allows LES-mode. In (b), $l_{\text{ratio}} > 1$ marks actually determined 'LES' region.

This sharp drop in the FSTI is not desired. Especially without an STG, one would require the model to convect the modelled turbulence throughout the passage, as the RANS-γ model does. An explanation for the strong decrease can be found in the shielding function f_d and the corresponding length scale ratio. We exemplarily present the 2D contour plots for DDES-γ in Fig. 10. Remembering the definition of l_{DDES} (see Eq. (3)) and physical meaning of l_{ratio} (see Eq. (6)), it becomes clear, that the distinct $f_d = 1$ region in the free-stream in combination with high l_{ratio} values is the origin of the strong reduction of modelled TKE. The shielding function, spuriously, enables an LES-mode with $f_d = 1$ and the utilized SLS approach by Shur et al. [24] determines very small Δ_{SLS}, which yield a strong reduction of modelled TKE. Generally, it is not desired to have this unphysical reduction without any opportunity of filling this gap with resolved scales in the free-stream, which becomes even worse when simulating multi-row or multi-stage configurations.

The presented results emphasize, that the coupled DDES-γ model is superior to the original DDES-FT model. A combination with an underlying transition model suppresses undesired premature TKE and leads to improved transition prediction. Nonetheless, the baseline DDES setup (*dynamic* solver blending and *no* STG) does also show weaknesses such as predicting bypass transition and preserving modelled FSTI. In the following subsections, we will consider different setups and discuss their impact only on DDES-γ simulations.

2. Assessment of the effect of STG for DDES-γ

After we analyzed the baseline DDES setup in the previous subsection and worked out differences between the fully turbulent and transitional approach, we now assess the impact of synthetic turbulence. Within this subsection, we run the DDES-γ model *without* and *with* STG, in the following referred to as DDES-γ and DDES-γ-STG respectively. Still, the *dynamic* solver blending is utilized. Details about the STG setup can be found in Sec. III.A.

We start with the visualization of the friction coefficient c_f in Fig. 11. Focusing the suction side (cf. Fig. 11a) first, the effect of STG is limited to the region of transition and reattachment. Small improvements in terms of a reattachment further upstream are visible and the c_f value after reattachment show better agreement with the DNS data. The surface values do not seem to be affected strongly by resolved scales in the free-stream. Fig. 12 shows boundary layer cuts of the resolved TKE on the suction side. The incoming resolved turbulence is apparent from the first station for DDES-γ-STG and in good agreement with our LES simulation, while DDES-γ does not determine any resolved content. Interestingly enough, the circumstances prior to separation are predicted almost identical by both approaches, as can be seen in the friction coefficient (cf. Fig. 11a) and also with velocity boundary layer profiles (not shown here). At the transition onset (at $x/c_{\text{ax}} \approx 0.6$), both model approaches show a sudden increase of maximum resolved TKE. While DDES-γ-STG slightly over-predicts k_{res}, DDES-γslightly underestimates the level of LES. The minor over-prediction of resolved turbulence by DDES-γ-STG is the origin for the better agreement with LES results because the increased turbulence level yields an earlier closure of the separation bubble, as can be seen in Fig. 11a. Generally, taking STG into account, is beneficial for the prediction of separation-induced transition since the k_{res} profiles are in fair agreement with our LES results.

Circumstances on the pressure side, as shown in Fig. 11b, require further attention. For the bypass transition, the synthetic turbulence from the free-stream, shows no actual impact. The transition onset is slightly shifted upstream towards other DDES or DNS reference data, but this effect seems to be negligible. A potential reason for this lies in the

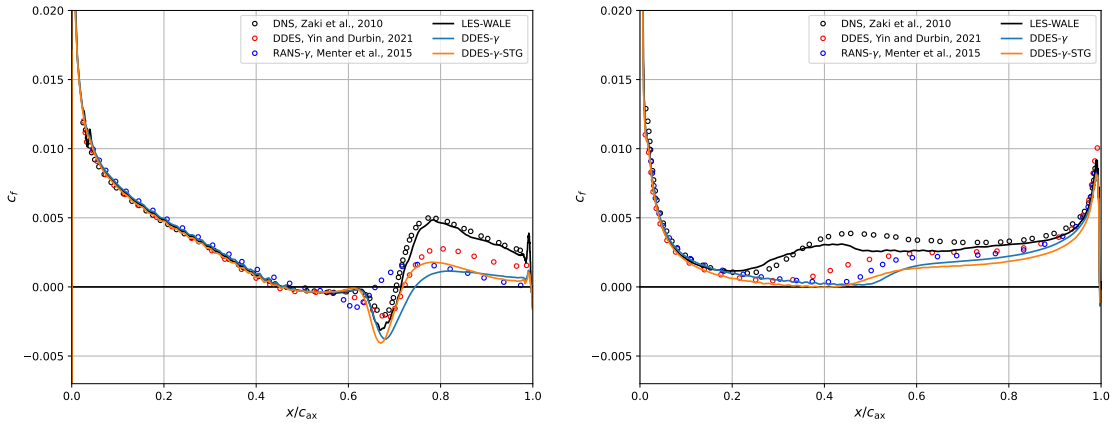

(a) Suction side **(b) Pressure side**

Fig. 11 Friction coefficient c_f along respective blade sides.

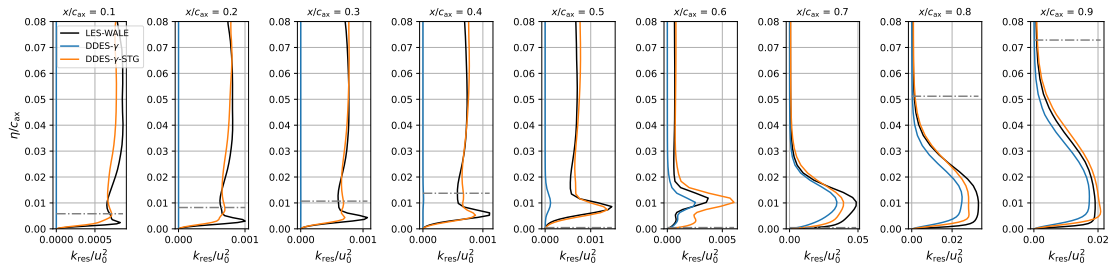

Fig. 12 Normalized wall-normal boundary layer cuts of resolved TKE along the suction side. Horizontal grey dash-dotted line depicts the boundary layer edge for our LES reference simulation.

DDES-γ model design. It needs to be remembered, that judging the transition process only by surface values such as c_f may lead to wrong conclusions. In the closest wall-vicinity, the shielding function f_d prevents any consideration of resolved scales due to f_d equal to zero (as can be seen in Fig. 13). $f_d = 0$ enforces RANS-mode in this region and, hence, the impact of resolved scales is diminished. This is intended for the original DDES model concept, but for a simulation with STG this behavior is potentially not desired. If resolved scales are provided with an STG, the mesh is most likely designed sufficiently fine enough in the wall-vicinity and, hence, a boundary layer shielding might not be required.

A more comprehensive assessment of the accurate prediction of the transition process on the pressure side is facilitated by the extraction of maximum modelled and resolved TKE for each streamwise boundary layer cut and

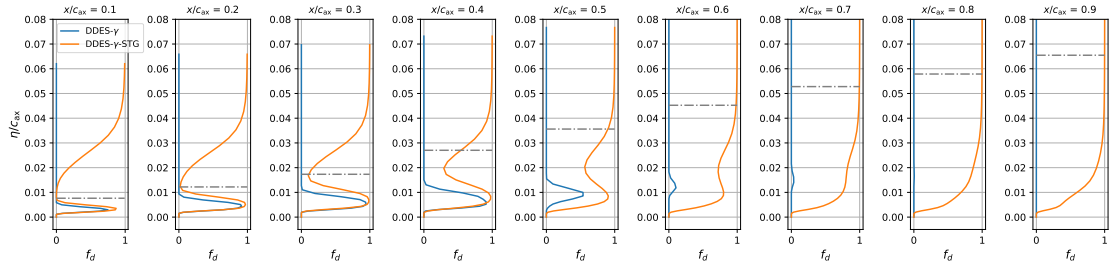

Fig. 13 Wall-normal boundary layer cuts of the shielding function f_d along the pressure side. Horizontal grey dash-dotted line depicts the boundary layer edge for our LES reference simulation.

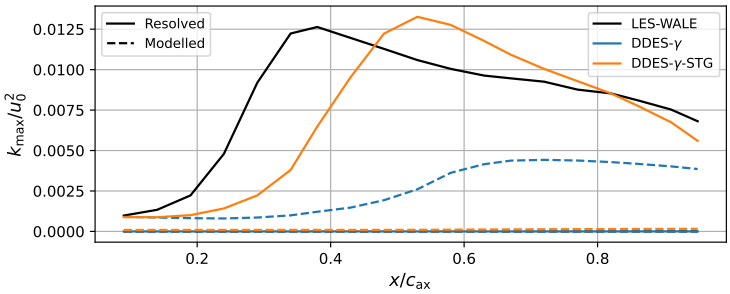

Fig. 14 Extracted maximum modelled and resolved TKE at streamwise boundary layer cuts on the pressure side.

plotting these values along the normalized x-axis. Results for the comparison of DDES-γ and DDES-γ-STG can be found in Fig. 14. Since the boundary layer cuts also consider the flow state away from the wall, a more complete picture of the transition process can be captured. Now, the effect of the STG is more apparent. The simulation without resolved scales does not follow the trend of LES and the transition process is predicted by modelled TKE, which can be seen in the increase of k_{mod} between $x = 0.5 - 0.65c_{\mathrm{ax}}$. For DDES-$\gamma$-STG, the trend is positive and bypass transition is now captured by resolved scales (see increase between $x = 0.3 - 0.55c_{\mathrm{ax}}$), but, still, there are deviations in comparison to LES visible. A global shift towards a delayed transition can be seen, which potentially has its origin in the coarser mesh resolution of the DDES simulation. The overall level of resolved TKE k_{res} is lower at the upstream stations on the pressure side, which yields this shift in Fig. 14.

The previously mentioned issue of unnatural decay of FSTI needs to be assessed for the STG setup. The visualization of modelled, resolved and total TI in Fig. 15 confirms a positive impact of the STG on the FSTI. We already saw the strong decay of modelled, and thus, also total TKE for DDES-γ. For the simulation with STG, we see good agreement with numerical reference DNS data. We fitted the decay of k_{res} (cf. Fig. 15b) to meet the DNS data. The sum $(k_{\mathrm{mod}} + k_{\mathrm{res}})$ in Fig. 15c yields a slight over-prediction, which we still accept as suitable for this case. Since we now have

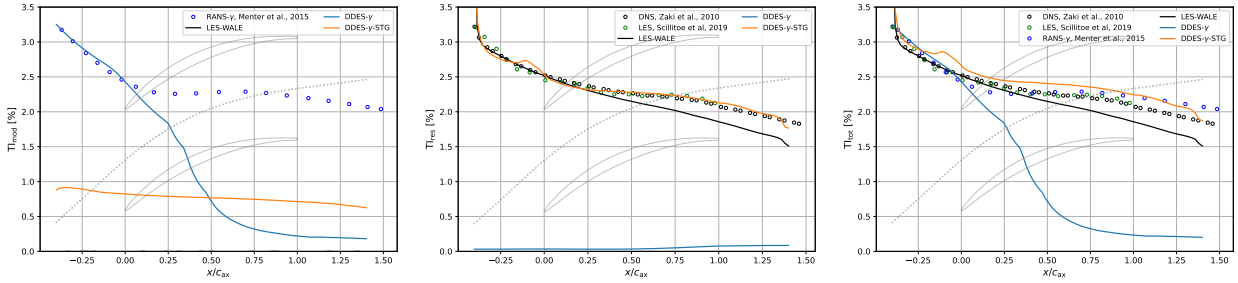

(a) Modelled component **(b) Resolved component** **(c) Modelled + resolved component**

Fig. 15 Turbulence intensity TI along extracted streamline intersecting the leading edge mid-pitch position (illustrated in the background with grey dots).

resolved content in the free-stream, it is acceptable, that the shielding function f_d (see Fig. 16b) globally determines values equal to unity. A reduction of modelled TKE is balanced by the resolved scales and even the modelled content is not reduced for DDES-γ-STG as can be seen in Fig. 15a. Fig. 15 and Fig. 16 show the positive effect of resolved turbulence on a more favorable shielding function and the FSTI.

The general impact of STG is illustrated in this subsection. When only focusing on surface values, the impact of resolved scales is small, even though the DDES-γ results *with* STG generally come closer to the DNS reference data. Assessing the transition process, specifically on the pressure side, by analyzing the total turbulence level, a positive effect of STG can be seen. Further, the free-stream is handled more consistently which means the prescribed turbulence is convected throughout the passage without unphysical decay.

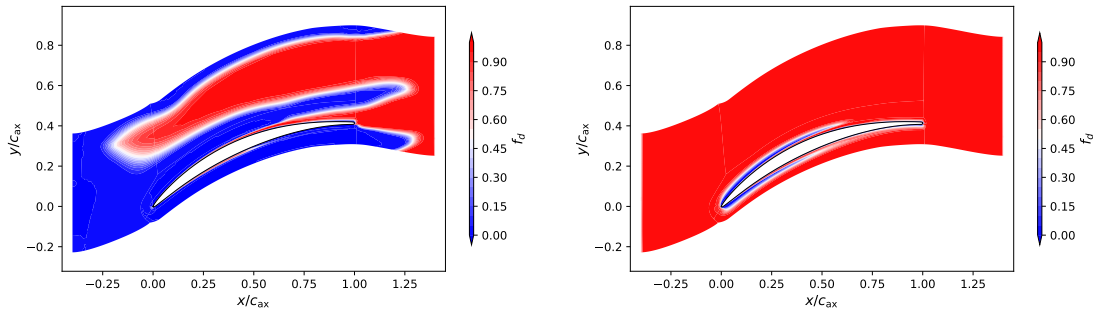

(a) DDES-γ **(b) DDES-γ-STG**

Fig. 16 Time-averaged contour slice of spanwise-averaged shielding function. $f_d = 0$ denotes the RANS region (blue), $f_d = 1$ allows a length scale comparison, hence, marks the region of potential LES-mode (red).

3. Variation of inviscid flux blending for DDES-γ with STG

Previously shown results with DDES-γ and the STG are promising but also show minor deviations when focusing on the surface value c_f. In this subsection, we vary the numerical solver blending (described in Sec. II.B) while utilizing the STG. Yin and Durbin [15] also applied a *constant* solver blending (they used an amount of 25 % upwind scheme) to avoid undesired numerical oscillations. For the utilized solver settings (described in Sec. III.A), we defined a constant upwind amount of $\sigma_b = 5$ %. In the following, results of DDES-γ with *dynamic* solver blending are labeled as DDES-γ-dyn, whereas results of the 5 % *constant* solver blending will be named DDES-γ-const.

To illustrate the differences between *dynamic* and *constant* solver blending, we show boundary layer cuts of the blending factor in Fig. 17. While the *dynamic* approach derives the blending factor based on the flow physics and model specific parameters, the *constant* factor is simply visualized for orientation purposes. We learn, that on both blade sides, the *dynamic* blending determines a region of $\sigma_b = 1$ in the boundary layer which marks a fully upwind region. This more dissipative solver scheme in the boundary layer has direct impact on physical results and affects the prediction of the transition processes negatively. Fig. 18 confirms these findings. The separation-induced transition on the suction

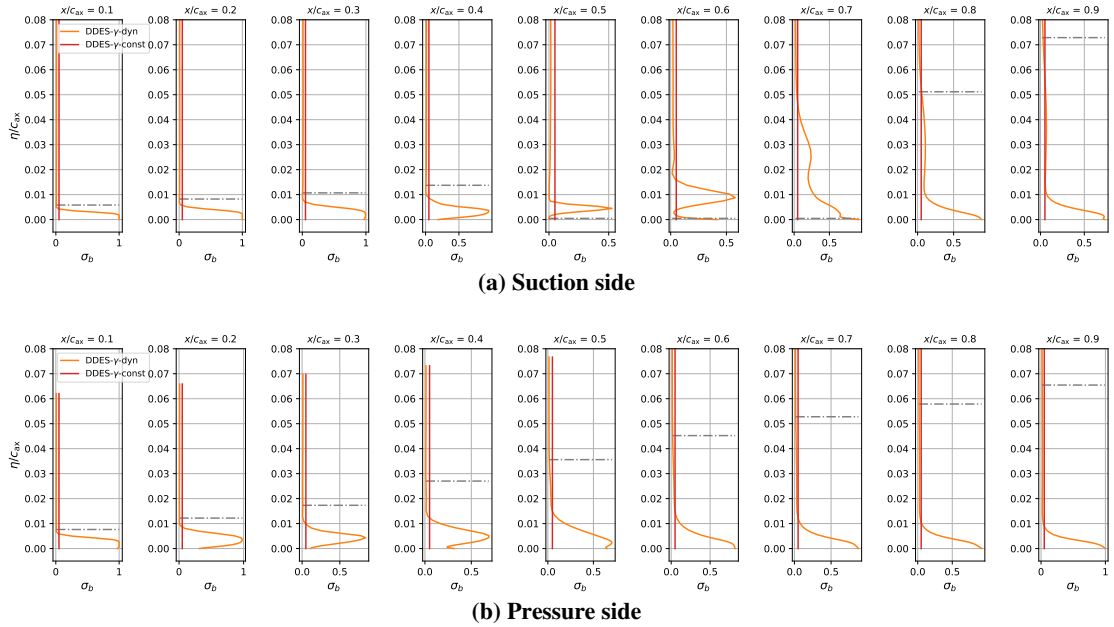

(a) Suction side

(b) Pressure side

Fig. 17 Boundary layer cuts of the solver blending factor on both blade sides separately. Horizontal grey dash-dotted line depicts the boundary layer edge for our LES reference simulation.

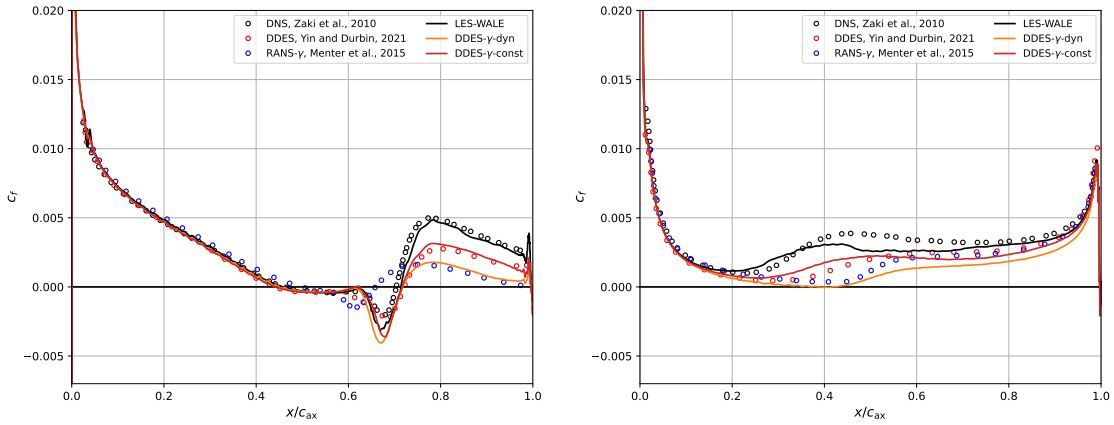

(a) Suction side **(b) Pressure side**

Fig. 18 Friction coefficient c_f along respective blade sides.

side (cf. Fig. 18a) and bypass transition on the pressure side (cf. Fig. 18b) has been predicted more accurately by the DDES-γ-const. On both sides, we see good agreement with DDES results of Yin and Durbin [15] and a closer shift towards DNS reference data. The improvements on the pressure side need to be emphasized. While DDES-γ-dyn shows big deviations to reference data, results with a constant solver blending are remarkably improved and closer to DNS reference data.

The effect of a higher amount of upwind scheme in the boundary layer can be shown with k_{res} boundary layer cuts in Fig. 19. On the suction side in Fig. 19a, we see only small deviations. Improvements by the *constant* blending approach are mostly apparent at stations $0.4 \leq x/c_{\text{ax}} \leq 0.7$, where results are moving closer to LES data. The pressure side (cf. Fig. 19b) shows bigger differences between these two blending approaches. It becomes clear, that the *constant* solver blending results follow LES reference data even at upstream locations, whereas the *dynamic* approach underestimates resolved TKE. These results show the sensitivity of the transitional process to the numerical dissipation, controlled by

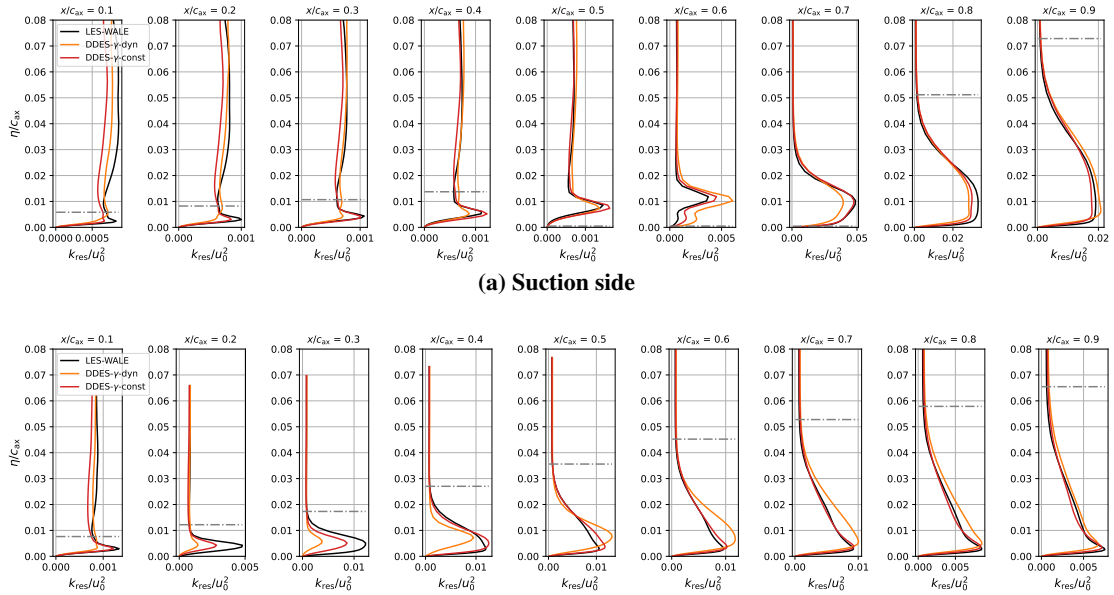

(a) Suction side

(b) Pressure side

Fig. 19 Boundary layer cuts of the normalized resolved TKE on both blade sides separately. Horizontal grey dash-dotted line depicts the boundary layer edge for our LES reference simulation.

the solver blending *with* an utilized STG. We also varied the solver blending for setups *without* the STG (not shown in this work), but results were aligned with those of DDES-γ-dyn, which furthermore emphasizes the interdependency of resolved scales, coming from the STG, and the numerical dissipation, controlled by the solver blending approach.

A critical comment on this could be, that the bypass transition process now relies on resolved turbulence and is predicted by resolved scales. We obtain improved results with DDES-γ and the *constant* solver blending, but it is questionable if we are still in the originally intended application range or if the model now acts more like an LES model. We already commented on this in the methodology section (cf. Sec. II.C). Moreover, the choice of the *constant* blending factor (here 5 %) can be seen as another adjustable model parameter. We saw, that with the constant factor, the resolved turbulence is controlled and increased by less dissipation in the boundary layer. It cannot be said, that this factor will stand the test of time, because different test cases or rather modified mesh resolutions will yield other dissipative properties and the value of 5 % might be adjusted. This needs to be kept in mind, when finally evaluating these results. Generally, the DDES-γ model with a *constant* solver blending shows improved results and reference data is met with acceptable accuracy.

IV. Conclusion and outlook

We gave an overview of the recently published transitional DDES approaches and motivated why this topic is relevant for the turbomachinery design process. After that, our coupled DDES-γ model was introduced and the model behavior was discussed theoretically. The model's performance in flows featuring both separation-induced and bypass transition was assessed with the compressor cascade V103, whereas the analysis is structured in three different subsections. The main findings can be summarized as follows:

- The comparison of baseline (= *dynamic* solver blending and *no STG*) DDES-FT and DDES-γ illustrated the strength of incorporating a transition model to predict transitional flows. While DDES-FT mainly failed to predict both transition types, we saw improvements for DDES-γ. The prediction of bypass transition with DDES-γ does not follow the reference data. But we could also work out, that this cannot be expected from a model approach, which treats the attached boundary layer with RANS-mode and does not include any resolved content. As a weakness of DDES-γ, we found unintended decay of modelled FSTI for the baseline configuration.
- When integrating STG, further improvements could be achieved. The FSTI is now maintained and in good agreement with reference data. Furthermore, the prediction of the separation-induced transition has been improved, whilst in the reattachment region we still see minor deviations. Only moderate improvement on the prediction of the bypass transition (if assessing surface values) could be explained with the model design. The shielding function f_d forces a RANS-mode in the closest wall-vicinity, which is why no big impact of resolved scales on the friction coefficient c_f could be recognized. When judging the transition process based on boundary cuts of the resolved TKE, beneficial behavior of DDES-γ-STG could be shown.
- We, eventually, varied the solver blending (*dynamic* vs. *dynamic*). It could be seen, that the *constant* solver blending has a positive impact on the prediction of both transition types. The combination of resolved turbulence (STG) and a reduced amount of upwind fluxes in wall-vicinity allowed DDES-γ-const to capture the separation-induced transition and also remarkably improved the prediction of bypass transition. The sensitivity to numerical dissipation (meaning a switch from *dynamic* to *constant* solver blending) is only given for the setup with an utilized STG.

The general strength of the DDES-γ could be illustrated and we showed, that an accurate prediction of the transition processes on both blade side is possible. At the same time, we critically discussed the concept of DDES-γ and obtained results.

Future work will focus on more complex configurations, such as fully-3D compressor cascades and multi-row/multi-stage setups. Especially for the latter, an assessment the predictive quality of wake-induced transition is required. The interaction of two rows will always yield an incoming wake for the downstream row. Therefore, DDES-γ needs to be assessed.

Acknowledgments

This research did not receive any specific grant from funding agencies in the public, commercial or non-for-profit sectors. All simulations have been carried out on DLR's supercomputer CARA[§] within the internal DLR project ADaMant[¶]. Eventually, we gratefully thank our colleagues at the Department, especially Michael Bergmann, Marcel Matha and Pierre Sivel, who spent a lot of time for discussions on this test case and the presented model.

Nomenclature

Abbreviations

DES	detached-eddy simulation	**LES**	large-eddy simulation
DDES	delayed detached-eddy simulation	**RANS**	Reynolds-averaged Navier-Stokes
DNS	direct numerical simulation	**SLS**	sub-grid length scale
FSTI	free-stream turbulence intensity	**STG**	synthetic turbulence generator
FT	fully turbulent	**TKE**	turbulent kinetic energy
HRL	hybrid RANS/LES		

Latin symbols

$c_{\mathbf{ax}}$	axial chord length	$\tilde{P}_k, D_k$	production and destruction term of modelled TKE
c_f	friction coefficient	P_γ, D_γ	production and destruction term of intermittency factor
c_p	pressure coefficient	t	time
d	distance to the next viscous wall	u_i, u_j	velocity vector
f_d	Spalart's shielding function	$u_{\mathbf{tang}}$	tangential velocity
k	turbulent kinetic energy	x_i, x_j	coordinate vector
l	length scale		

Greek symbols

γ	intermittency factor	μ_t	eddy viscosity
$\Delta_{\mathbf{SLS}}$	sub-grid length scale	ρ	density
η	wall-normal distance	σ_b	solver blending factor
μ	molecular viscosity	ω	turbulent dissipation rate

References

[1] Lardeau, S., Leschziner, M., and Zaki, T., "Large Eddy Simulation of Transitional Separated Flow over a Flat Plate and a Compressor Blade," *Flow, Turbulence and Combustion*, Vol. 88, No. 1-2, 2011, pp. 19–44. https://doi.org/10.1007/s10494-011-9353-0, URL https://link.springer.com/article/10.1007/s10494-011-9353-0.

[2] Marty, J., "Numerical investigations of separation-induced transition on high-lift low-pressure turbine using RANS and LES methods," *Proceedings of the Institution of Mechanical Engineers, Part A: Journal of Power and Energy*, Vol. 228, No. 8, 2014, pp. 924–952. https://doi.org/10.1177/0957650914548741.

[§]Link to technical specifications

[¶]Link to project homepage

[3] Scillitoe, A. D., Tucker, P. G., and Adami, P., "Large Eddy Simulation of Boundary Layer Transition Mechanisms in a Gas-Turbine Compressor Cascade," *Journal of Turbomachinery*, Vol. 141, No. 6, 2019. https://doi.org/10.1115/1.4042023.

[4] Magagnato, F., Pritz, B., and Gabi, M., "Comparison of DES and LES on the Transitional Flow of Turbine Blades," *Notes on Numerical Fluid Mechanics and Multidisciplinary Design*, Springer Berlin Heidelberg, 2007, pp. 212–221. https://doi.org/10.1007/978-3-540-77815-8_22, URL https://link.springer.com/chapter/10.1007/978-3-540-77815-8_22.

[5] Spalart, P., Jou, W.-H., Strelets, M., and Allmaras, S., "Comments on the feasability of LES for wings, and on a hybrid RANS/LES approach," *Computer Science*, 1997.

[6] Wang, L., Fu, S., Carnarius, A., Mockett, C., and Thiele, F., "A modular RANS approach for modelling laminar–turbulent transition in turbomachinery flows," *International Journal of Heat and Fluid Flow*, Vol. 34, 2012, pp. 62–69. https://doi.org/10.1016/j.ijheatfluidflow.2012.01.008.

[7] Wang, L., Mockett, C., Fu, S., and and, F. T., "Turbomachinery flow simulations using a hybrid RANS/LES method combined with a RANS transition model," *Proceedings XXI International Symposium on Air Breathing Engines: ISABE Conference Busan, Korea*, 2013. URL https://dlr-bibliothekskatalog.bsz-bw.de/cgi-bin/koha/opac-detail.pl?biblionumber=173698&query_desc=kw,wrdl:hybridransles.

[8] Xiao, Z., Wang, G., Yang, M., and Chen, L., "Numerical investigations of hypersonic transition and massive separation past Orion capsule by DDES-Tr," *International Journal of Heat and Mass Transfer*, Vol. 137, 2019, pp. 90–107. https://doi.org/10.1016/j.ijheatmasstransfer.2019.03.119.

[9] Wang, L., and Fu, S., "Modelling flow transition in a hypersonic boundary layer with Reynolds-averaged Navier-Stokes approach," *Science in China Series G: Physics, Mechanics and Astronomy*, Vol. 52, No. 5, 2009, pp. 768–774. https://doi.org/10.1007/s11433-009-0047-8.

[10] Sørensen, N. N., Bechmann, A., and Zahle, F., "3D CFD computations of transitional flows using DES and a correlation based transition model," *Wind Energy*, Vol. 14, No. 1, 2011, pp. 77–90. https://doi.org/10.1002/we.404.

[11] Sa, J. H., Cho, K. W., and Park, S. H., "Numerical Study of Blending Hybrid RANS/LES Method and γ-Re_θ Transition Model for Unsteady Turbulent Flow Analysis," *The 2016 Structures Congress (Structures16)*, 2016.

[12] Alam, M., Walters, D., and Thompson, D., "A transition-sensitive hybrid RANS/LES modeling methodology for CFD applications," *51st AIAA Aerospace Sciences Meeting including the New Horizons Forum and Aerospace Exposition*, 2013. https://doi.org/10.2514/6.2013-995.

[13] Walters, D. K., Bhushan, S., Alam, M. F., and Thompson, D. S., "Investigation of a Dynamic Hybrid RANS/LES Modelling Methodology for Finite-Volume CFD Simulations," *Flow, Turbulence and Combustion*, Vol. 91, No. 3, 2013, pp. 643–667. https://doi.org/10.1007/s10494-013-9481-9, URL https://link.springer.com/article/10.1007/s10494-013-9481-9.

[14] Yin, Z., Ge, X., and Durbin, P., "Adaptive detached eddy simulation of transition under the influence of free-stream turbulence and pressure gradient," *Journal of Fluid Mechanics*, Vol. 915, 2021. https://doi.org/10.1017/jfm.2021.117.

[15] Yin, Z., and Durbin, P. A., "Detached Eddy Simulation of Transition in Turbomachinery: Linear Compressor Cascade," *Journal of Turbomachinery*, Vol. 144, No. 3, 2021. https://doi.org/10.1115/1.4052309.

[16] Möller, F. M., Tucker, P. G., Wang, Z.-N., Morsbach, C., and Bergmann, M., "On the Prediction of Separation-Induced Transition by Coupling Delayed Detached-Eddy Simulation with γ-Transition Model," *15th European Conference on Turbomachinery Fluid dynamics & Thermodynamics*, ETC, 2023.

[17] Mayle, R., "The role of laminar-turbulent transition in gas turbine engines," *Transactions of the ASME*, 1991.

[18] Travin, A., Shur, M., Strelets, M., and Spalart, P. R., "Physical and Numerical Upgrades in the Detached-Eddy Simulation of Complex Turbulent Flows," *Fluid Mechanics and Its Applications: Advances in LES of Complex Flows*, Springer Netherlands, 2002, pp. 239–254. https://doi.org/10.1007/0-306-48383-1_16, URL https://link.springer.com/chapter/10.1007/0-306-48383-1_16.

[19] Spalart, P. R., Deck, S., Shur, M. L., Squires, K. D., Strelets, M. K., and Travin, A., "A New Version of Detached-eddy Simulation, Resistant to Ambiguous Grid Densities," *Theoretical and Computational Fluid Dynamics*, Vol. 20, No. 3, 2006, pp. 181–195. https://doi.org/10.1007/s00162-006-0015-0.

[20] Gritskevich, M. S., Garbaruk, A. V., Schütze, J., and Menter, F. R., "Development of DDES and IDDES Formulations for the k-ω Shear Stress Transport Model," *Flow, Turbulence and Combustion*, Vol. 88, No. 3, 2011, pp. 431–449. https://doi.org/10.1007/s10494-011-9378-4.

[21] Chauvet, N., Deck, S., and Jacquin, L., "Zonal Detached Eddy Simulation of a Controlled Propulsive Jet," *AIAA Journal*, Vol. 45, No. 10, 2007, pp. 2458–2473. https://doi.org/10.2514/1.28562.

[22] Probst, A., and Reuß, S., "Progress in Scale-Resolving Simulations with the DLR-TAU Code," *Deutscher Luft- und Raumfahrtkongress*, 2016.

[23] Mockett, C., Fuchs, M., Garbaruk, A., Shur, M., Spalart, P., Strelets, M., Thiele, F., and Travin, A., "Two Non-zonal Approaches to Accelerate RANS to LES Transition of Free Shear Layers in DES," *Progress in Hybrid RANS-LES Modelling*, Springer International Publishing, 2015, pp. 187–201. https://doi.org/10.1007/978-3-319-15141-0_15.

[24] Shur, M. L., Spalart, P. R., Strelets, M. K., and Travin, A. K., "An Enhanced Version of DES with Rapid Transition from RANS to LES in Separated Flows," *Flow, Turbulence and Combustion*, Vol. 95, No. 4, 2015, pp. 709–737. https://doi.org/10.1007/s10494-015-9618-0.

[25] Menter, F. R., Smirnov, P. E., Liu, T., and Avancha, R., "A One-Equation Local Correlation-Based Transition Model," *Flow, Turbulence and Combustion*, Vol. 95, No. 4, 2015, pp. 583–619. https://doi.org/10.1007/s10494-015-9622-4.

[26] Roe, P., "Approximate Riemann solvers, parameter vectors, and difference schemes," *Journal of Computational Physics*, Vol. 43, No. 2, 1981, pp. 357–372. https://doi.org/10.1016/0021-9991(81)90128-5.

[27] Shur, M. L., Spalart, P. R., Strelets, M. K., and Travin, A. K., "Synthetic Turbulence Generators for RANS-LES Interfaces in Zonal Simulations of Aerodynamic and Aeroacoustic Problems," *Flow, Turbulence and Combustion*, Vol. 93, No. 1, 2014, pp. 63–92. https://doi.org/10.1007/s10494-014-9534-8.

[28] Morsbach, C., and Franke, M., "Analysis of a synthetic turbulence generation method for periodic configurations," *ERCOFTAC Workshop Direct and Large-Eddy Simulation 11*, Springer, 2017.

[29] Matha, M., Morsbach, C., and Bergmann, M., "A comparison of methods for introducing synthetic turbulence," *7th European Conference on Computation Fluid Dynamics*, 2018.

[30] Hilgenfeld, L., and Pfitzner, M., "Unsteady Boundary Layer Development Due to Wake Passing Effects on a Highly Loaded Linear Compressor Cascade," *Journal of Turbomachinery*, Vol. 126, No. 4, 2004, pp. 493–500. https://doi.org/10.1115/1.1791290.

[31] Zaki, T. A., Wissink, J. G., Rodi, W., and Durbin, P. A., "Direct numerical simulations of transition in a compressor cascade: the influence of free-stream turbulence," *Journal of Fluid Mechanics*, Vol. 665, 2010, pp. 57–98. https://doi.org/10.1017/s0022112010003873.

[32] Nicoud, F., and Ducros, F., "Subgrid-Scale Stress Modelling Based on the Square of the Velocity Gradient Tensor," *Flow, Turbulence and Combustion*, Vol. 62, No. 3, 1999, pp. 183–200. https://doi.org/10.1023/a:1009995426001.